THE EFFECT OF CROSSWIND ON ENGINE INGESTION DURING TAKEOFFS FROM WATER CONTAMINATED RUNWAYS

Joop H.M. Gooden
National Aerospace Laboratory NLR
Joop.Gooden@nlr.nl

Abstract

A method is developed for calculating the spray generated by tyres on water-contaminated runways and the resulting precipitation drag and engine ingestion. The method is based on droplet trajectory calculations. The initial conditions for these are based on (semi) empirical relations. The spray is then calculated using a Monte Carlo approach with variations on the initial spray conditions. The calculation of the spray takes into account partial reflection on the aircraft surface and the flow of the remaining water film along the surface.

The method, named 'CRspray', has been validated using laboratory and flight test experiments. Contaminated runway drag and ingestion can be determined depending on the pool depth, wind conditions, aircraft geometry, tyre geometry and pressure, aircraft weight and the wing lift.

This paper deals specifically with crosswind-effects on the spray. Crosswind may lead to high engine ingestion rates, exceeding ingestion limits. This may cause engine performance decrease, but at excessive ingestion quantities also surge, stall or even flame-out may occur. The airworthiness requirements state that an airplane may not ingest hazardous quantities of water or slush into engines and APUs during takeoff, landing and taxiing. Therefore, evaluating the crosswind effects on contaminated runway operation is inevitable.

1 Introduction

A runway is considered contaminated by water if more than 25% of the used runway surface contains water with a pool depth of at least 3 mm. For airworthiness certification, pool depths up to 15 mm to 19 mm are considered [1],[2],[3],[4]. An aircraft taking off from a runway contaminated by standing water experiences both increased drag due to the displacement of the water by the tyres and due to the impingement of the water spray on the aircraft. This will result in a longer take-off run.

A good aircraft design avoids engine water ingestion. However, cross wind may deflect the spray towards the engine intake. Therefore, crosswind may lead to high engine ingestion rates, exceeding engine ingestion limits. This may not only cause engine performance decrease, but at excessive ingestion quantities also surge, stall or even flame-out may occur. As the aircraft already experiences an increased precipitation drag it is clear that the loss of an engine in this situation is critical. The airworthiness requirements state that an airplane engine or APU may ingest water but not in hazardous quantities during takeoff, landing and taxiing and that crosswind effects have to be examined in order to specify crosswind operation limitations to be included in the flight manual.

Therefore it is advisable to get a good impression on the properties of a given aircraft design both in terms of precipitation drag and engine water ingestion. This may affect the choice of undercarriage configuration, aircraft tyres but even the shape of the fuselage belly or the engine position.

Some simple methods exist to give an estimate of the precipitation drag. However, these methods unfortunately are only capable of giving a first rough estimate of the location of the spray and the magnitude of the precipitation

drag. Also the spray location is only roughly predicted and no information can be obtained on engine water ingestion. Moreover, cross wind effects can generally not be determined.

This fact urged the development of a more advanced method for prediction of the water contamination effects on aircraft performance. Therefore NLR developed a method called 'CR*spray*' ('Contaminated Runway Spray'). The method is based on water droplet trajectory calculations. The calculation uses a Monte-Carlo simulation and starts from basic principles supplemented with empirical data. The method has been validated using laboratory and flight test results.

This approach allows to vary parameters that affect the spray development and – as a consequence – airplane performance and safety. Among those is the effect of crosswind. Normally pool tests are only performed for the prevailing wind conditions. As the location of the spray sometimes is critical as far as engine ingestion is concerned, this does not give unambiguous information on the risks of engine ingestion in case of crosswind conditions. Moreover, weather conditions provoking runway flooding will often go together with unfavorable wind conditions. Therefore it is inevitable to study the effects of wind on the spray development and ingestion risk.

The paper starts with a description of the method. Next, some validation results will be shown. Also the effect of changing some of the discussed parameters is focused on. Finally, the effects of crosswind on the spray will be highlighted for a typical aircraft configuration.

2. Spray pattern calculation

CR*spray* assumes the spray to be composed of a large number of single droplet trajectories. In order to start the trajectory calculation, initial values of particle properties: velocity vector, particle diameter and location are required. The initial properties are derived from empirical data available for water sprays, mainly the rudimentary ESDU spray description [5], on one hand and on basic, physical principles on the other hand.

A tyre rolling through a water pool develops a wave front because the water is washed away from the tyre track. If this happens with sufficient speed, the resulting wave contains so much energy that the water surface tension can no longer keep the wave integrated and particles start to separate into a spray. In front of the tyres a bow wave develops, ejecting spray in forward and upward direction. Besides and aft of the tyres a straight side wave front develops. For side-by-side tyres the sideways wave fronts in between the tyres merge and a single straight center-wave front develops from which the spray emerges in vertical direction.

The initial conditions are derived partly from the ESDU spray model. This model is too concise, however, to derive all the initial quantities for the droplet trajectory calculation. Moreover, it does not contain the important bow wave in front of the tyres. Another limitation of the ESDU model is that it assumes a linear downstream spray development, which can not be true for the actual spray as the vertical droplet velocity is not constant but changes due to gravity and aerodynamic resistance forces. Nevertheless, the ESDU data offer the advantage that spray-data of a relatively large number of different undercarriage and tyre combinations have been modeled. Therefore the ESDU data are used as a guide for the side wave front location and the initial velocity vector as well as the variance thereof. The latter two are determined indirectly from the spray envelopes available from the ESDU model. Other parameters (spray density, droplet size, bow wave properties) are modeled using spray data obtained by other researchers, both in model experiments ([6], [7], [8]) as well as flight tests by Dassault (Falcon 2000) [9], Saab (SAAB 2000) [10] and NLR (Cessna Citation II) [11],[12].

Disturbances in the flow field, e.g. caused by the circulation around the wing generated by wing lift or the wind are taken into account. The same is done for the airflow generated by the spray itself as a result of air entrainment.

2.1 Main initial parameters

A short survey of the initial parameters used is given here:

Hydroplaning reference speed:

The airworthiness regulations (AMJ 25X1591) define a maximum drag speed:

$$V_p = 17.6\sqrt{p_i}$$

(p_i tyre inflation pressure in bar, V_p in m/s).

Spray wave front location:

The location of the side wave front is related, but not equal to the position of the side wave front from the ESDU data as the ESDU data mainly focus on the most intense upper part of the spray and not on the ground bound part of the spray. This most intense part of the spray is represented by a parallelogram area, see figure 1.
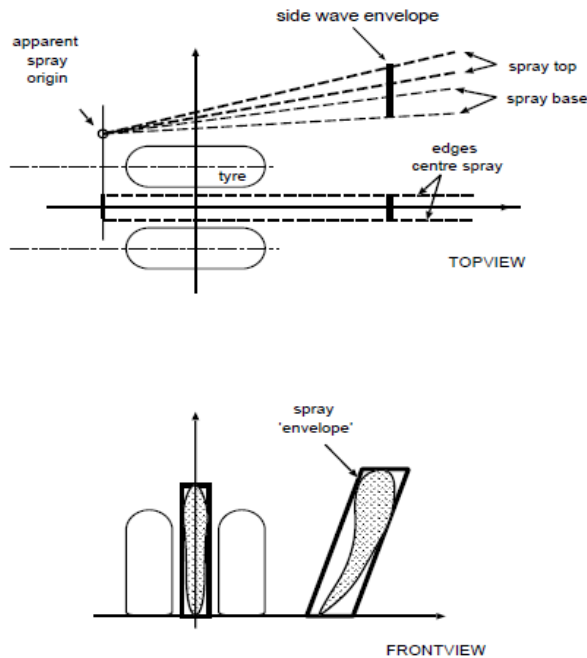
Fig. 1. ESDU spray schematization.

The bow wave front has an elliptical shape, with both halves split up by a straight connection in case of side-by-side tyres. On approaching the hydroplaning speed, the bow wave disappears. The centre wave front is a straight line, starting from the bow wave and running aft.

Particle initial velocity vector: The initial velocity vector is estimated, using the ESDU envelope as a starting point. Corrections are applied for the decay of the initial velocity at positions further downstream along the wave front.

Particle diameter:

The spray starts as a liquid sheet. Such a sheet injected into a gaseous environment normally is unstable. Oscillation of this sheet and subsequent break-up lead to atomization. First liquid ligaments (primary break up) and then droplets (secondary break up) are formed. Disintegration of larger droplets continues till the droplets become small enough such that the surface forces keep the droplets together. Therefore, droplet breakup is typified by the Weber number, representing the ratio of aerodynamic forces acting on the droplet to the stabilizing surface tension force.

$$We = \frac{\rho_a V_p^2 D_p}{\sigma_p} \qquad (1)$$

ρ_a equals the air density, V_p the particle velocity, D_p the particle diameter and σ_p the particle surface tension. If the We-number becomes smaller than a critical breakup value, droplets no longer disintegrate [13]. This value depends on the droplet slip velocity Reynolds number. Kolev [14] gives the following relation:

$$We_{bu} = 55\left(\frac{24}{Re} + \frac{20.1807}{Re^{0.613}} - \frac{16}{Re^{2/3}}\right)$$

This relation can be approximated very well on its validity range of 200<Re<2000 by the simpler expression:

$$We_{bu} = \frac{671}{Re^{0.63}} \qquad (2)$$

being used in CR*spray*. For Re> 2061, We_{bu} is taken equal to 5.48, the minimum value found for break up under sudden acceleration conditions. For Re<200 the equation is no longer valid. In that range particle diameters tend to become very large. It is shown in the literature (e.g.[16], [17]) that stable water droplets falling in air will likely break up if they become too large. The upper limit lies in the range of droplet diameters of 6 to 10 mm Therefore, the maximum *average* particle diameter has been limited to 8 mm.

Whether or not viscosity is important in this process is determined by the Ohnesorge number,

$$Oh = \frac{\mu_p}{\sqrt{\rho_p D_p \sigma_p}}$$

where μ_p stands for the particle dynamic viscosity. A higher Oh, i.e. viscosity, delays droplet breakup, resulting in a correction to We if $Oh<0.01$ [15]. For the sprays studied here viscosity effects may be disregarded.

Although the droplet size distribution normally seems to fit a Gaussian distribution in the natural log of the diameter [14], [15] CR*spray* applies the Gaussian distribution on D_p itself for simplicity.

<u>Atomization fraction</u>

Not all the water behind the wave front will be atomized. Part of it just moves sideways, especially further downstream. Therefore an atomization fraction parameter AF is introduced, being the ratio of water atomized by the wave front, relative to the total volume of water initially present in the same part of the pool through which that wave front passed. The local atomization fraction has been related empirically to the local Froude number and the local initial velocity magnitude. For this purpose the results in [6], [7] and [8] have been used.

2.2 Flow field velocity

Particle sizes in the spray typically range from 0.5 to 10 mm. A measure for describing the ability of a particle to follow the flow is given by the particle inertia parameter:

$$K = \frac{\rho_p D_p^2 V_R}{18 \mu_a c}$$

where ρ_p stands for the particle density, V_R equals the particle slip velocity, μ_a the dynamic viscosity of air and c a reference length scale. The particle inertia is reflected in the particle equation of motion as follows, see e.g. [18]:

$$K\ddot{\vec{\xi}} = \left(\frac{C_D Re}{24}\right)\vec{\omega}_D + \left(\frac{K}{Fr^2}\right)\frac{\vec{g}}{g}$$

with $\vec{\xi} = \frac{\vec{r}}{c}$ being the dimensionless location vector, $\vec{\omega}_D$ the dimensionless particle slip velocity $\frac{\vec{V}_R}{U_{ref}}$, $\vec{g}$ the gravitational vector and Fr the Froude number, $\frac{U_{ref}}{\sqrt{(gc)}}$

As described in [18], a study concerning the droplet collection efficiency of airfoils, particles no longer are able to follow the flow curvature close to wing leading edges for $K>1$. For the sprays considered in the present study, typical values of K are well above 1. This means that small scale velocity perturbations to the flow field need not be modeled, as the particles will not be able to respond to those. Therefore, it is not necessary to calculate the flow field around the airplane in detail. In the present model only the general circulation around the wing, the entrainment velocity generated by the spray and – evidently – the (cross)wind velocity have been modeled.

The effects of wing lift on the flow field were included by putting a vortex-sheet at the wing chord and calculating the resulting flow field. The sheet, stretching from 5 to 75 percent of the local wing chord c, has constant distributed vortex strength, such that the wing lift is represented correctly.

A large part of the spray passes underneath the wing. For a low-winged aircraft it is important to mirror the circulation into the ground surface, which increases the disturbance velocity especially below the wing. For e.g. the Cessna Citation, the ground surface is at around 1/3rd of the wing chord below the wing. This will lead to an extended region with relatively low-speed air below the wing.

No interaction between the droplets constituting the spray has been assumed in the sense of droplet collisions. However, an indirect particle interaction has to be taken into account. This is the air entrainment velocity generated by the spray itself. This entrainment is caused by the drag forces acting on the separate droplets, resulting in the air in the vicinity of the spray to move in the same direction as the spray. This, in turn, reduces the slip velocity, sensed by the particles, and therefore lowers the drag forces on them. As a result the spray will rise higher. Because of the high spray density, the entrainment effect is significant. It is modeled, assuming that the air entrainment velocity is proportional to both the local particle density and the particle drag.

The crosswind velocity distribution with height is approximated by means of a 1/7th

power law distribution. The wind velocity at Z=10 m height is used as a reference:

$$\frac{V_x}{V_{w,10}} = \left(\frac{Z}{10}\right)^{\frac{1}{7}}$$

For tail mounted engines the main interest is in crosswinds towards the fuselage on the side of the engine under investigation and not away from the fuselage. Moreover, as cross wind velocities are in the order of 10 to 20 knots, and rolling velocities are a factor 2 to 10 higher, the angle between the effective wind direction and the fuselage axis remains relatively small. Therefore the effect of the fuselage on the cross wind field is not taken into account.

2.3 Aircraft modelling

If the spray hits the aircraft it is partially reflected. As the calculation of the flow field does not require a detailed modeling of the aircraft, only that part of the aircraft has to be modeled to some detail that can possibly be hit by the water spray in order to allow for the reflection and subsequent impingement drag calculation. A number of elementary 'building blocks' has been defined, like cylinders, flat surfaces, a fuselage fairing cross section, a wing like cross section, etcetera. This allows a quick representation of the shape of the aircraft in more or less detail, as desired. Some examples can be found in the sketches in this paper.

2.4 Precipitation drag

The precipitation drag consists of two main components, displacement drag and impingement drag. The first one is the result of the work performed by the tyres breaking their way through the water pool. The second drag force is a result of the spray impinging on and flowing along the airframe. The displacement drag is calculated using a slightly modified ESDU method [19]. The modification involves a $1/V^3$ decay at velocities above hydroplaning instead of the $1/V^2$- behavior as taken by ESDU. The modification is believed to better represent the available experimental data as the latter would result in a constant displacement drag, which is not confirmed by the experimental

data. Besides, [19] shows a displacement drag error bandwidth of around 40%, which is substantial and leaves room for improvement.

To calculate impingement drag, the spray is considered to consist of separate particles that hit the aircraft. A partial elastic collision is assumed. Upon collision, the spray partly reflects off the surface. The remaining part adheres to the surface and forms a water film that flows aft over the aircraft. The two main forces that contribute to the impingement drag are the collision force occurring at the moment of reflection and the surface shear force caused by the water film flow along the surface. The collision force dominates at parts of the aircraft surface being normal to the direction of movement, like the wing leading edge. The water film shear drag force dominates at those parts of the surface being more or less parallel to the direction of movement. Although the contribution of the collision forces normally is larger, the water film shear force cannot be neglected, as will be shown later. Both drag contributions therefore have to be modeled. The method used for derivation of both forces has been explained in more detail in [20].
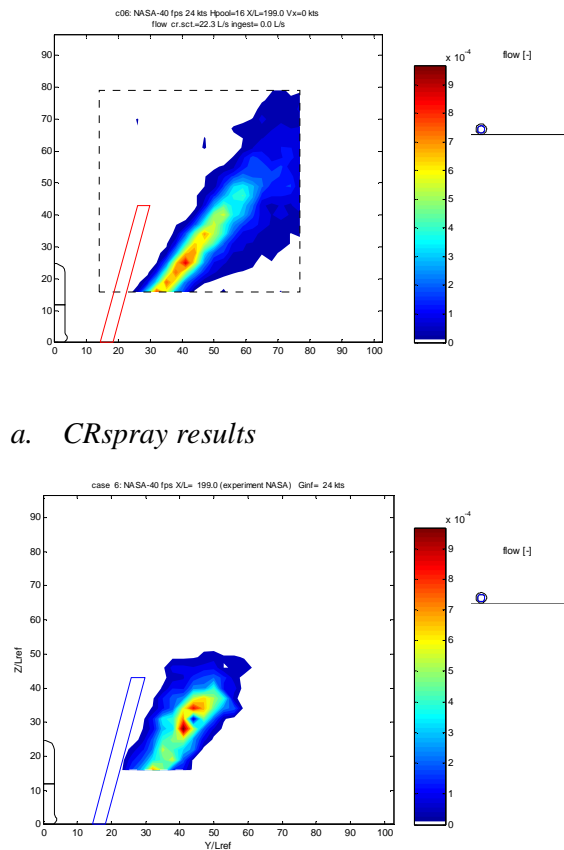
3. CR*spray* results

3.1 Validation

CR*spray* has been validated using both academic test cases as well as flight test results on a Cessna Citation II, the SAAB 2000 and the Dassault Falcon 2000. Also results obtained from a larger aircraft, the 100-seater Dassault Mercure, have been used. Comparisons with large transport type aircraft are still welcome to further validate the method for this category. Some results are shown here.

Figure 2 shows results for a test case given in [6]. That reference describes a number of tests on two different types of tyres with varying tyre pressures and tyre loads. The figure shows the results for a 26 inch cross-ply tyre, inflated to 3.1 bar. The tyre load amounts to 6700 N and the pool depth equals 16 mm. The ground speed equals 12.2 m/s (40 ft/s), corresponding to almost 70% of the hydroplaning velocity at the given tyre pressure. The parallelogram-shaped

ESDU envelope is also shown in figure 2. In this calculation 5000 particle tracks are used. Note that there is some discrepancy between the measured spray and the ESDU-envelope. Possibly this is caused because the tyre pressure used being only about 25% of the rated tyre pressure. A very reasonable comparison, not only in spray position, but also in spray density between CR*spray* and the experiment is obtained.


a.   CRspray results

b.   NASA measurement

Fig. 2. NASA test case: spray density at 5.06 m (16.6 ft) aft of tyre.

A comparison between calculation and a flight test, conducted by NLR, for the Cessna Citation II aircraft is shown in figure 3. The main gear has a single 22x8 cross-ply tyre. The nose gear is equipped with a single 18x4.4 cross-ply tyre, provided with chines. The main gear tyre pressure equals 9.6 bar (140 psi), the

nose gear pressure equals 8.4 bar (120 psi), resulting in hydroplaning velocities equal to 106 and 99 kts respectively, according to AMJ. Aircraft speed was 80 kts, about 70 % of the hydroplaning speed. The pool depth equaled 12 mm.

a. flight test
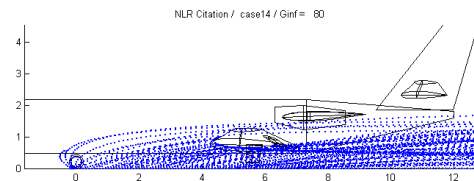
b. calculated nose gear spray
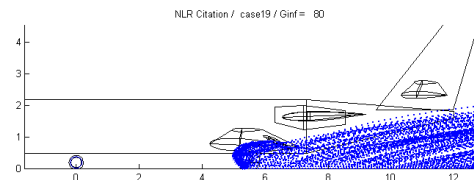
c. calculated main gear spray

Fig. 3. Cessna Citation II: comparison of measured and calculated spray pattern at 80 kts

During the flight tests, hydroplaning started to occur at speeds above 90 kts. Note that V_p according to AMJ is not equal to the actual velocity above which initial signs of hydroplaning occur, but roughly corresponds to the velocity were maximum tyre displacement drag is found. For instance, data from Leland and Taylor [21] shows that tyre spin down starts from a velocity of 8% below V_p.

Figure 4 shows the precipitation drag for this aircraft for the same pool depth (12 mm). In this case, the CR*spray*-prediction is performed using 2000 particles for each side spray. A test has been done to calculate the drag with a

varying number of particles and this learned that about 1000 particles per side spray are required to obtain a drag prediction accuracy within about 1% of the value obtained with a very large number of particles (10000). The figure shows that the predicted precipitation drag agrees well with the flight test data.
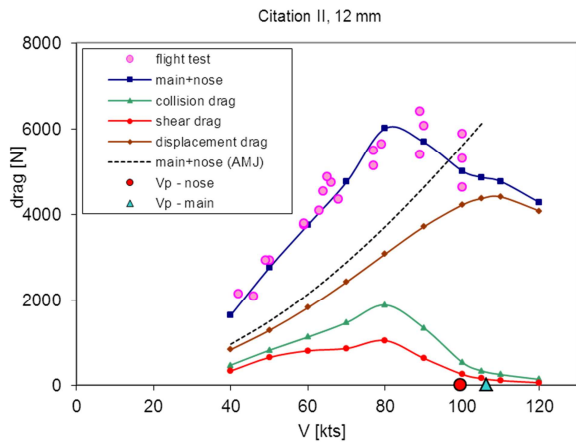

Fig. 4. Cessna Citation II: CR*spray-results, compared with flight test data and AMJ rule*

The figure also shows the AMJ drag prediction that is assumed to be valid below hydroplaning. This value is seen to be substantially lower than the flight test data. The AMJ drag prediction takes into account the displacement drag of each undercarriage and the impingement drag of the nose wheel by means of a relation between drag and wetted length of the fuselage. Apparently this relation is too crude. The cause for this difference may be that the relation was derived using data from larger aircraft. It is recognized generally that traditional methods may underpredict precipitation drag especially for smaller jet aircraft.

The separate drag contributions (shear drag, collision drag and displacement drag) are shown as well. The nose gear is the main contributor to the collision drag as much of this spray hits the lower side of the fuselage and the wing leading edges. It is seen that the shear drag cannot be neglected. It amounts to about 2/3rd of the collision drag.

As soon as hydroplaning appears, the spray becomes very flat and the magnitude of

impingement on the aircraft reduces significantly. Here the drag consists almost exclusively of displacement drag.
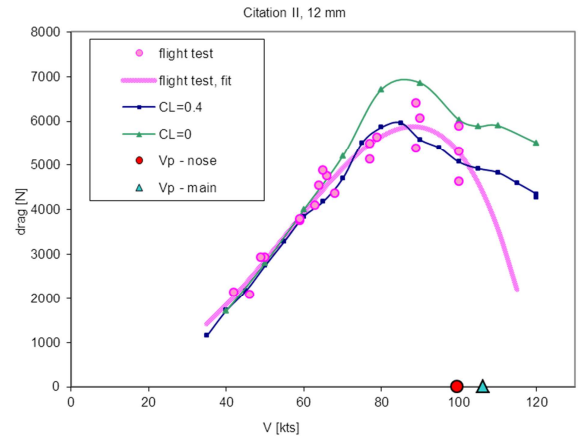

Fig. 5. Effect of wing lift on precipitation drag

CR*spray* enables studying the effect of changing some parameters on the precipitation drag. The influence of wing lift and tyre pressure is shown here. For the Citation normally C_L=0.4 is assumed during the take-off run. A calculation has been performed for zero lift as well. This increases the tyre load, and reduces the induced velocity field around the wing. Figure 5 shows the effects on the drag. It is clear that the differences will increase with velocity as the wing lift develops. The higher tyre load results in a more dense spray and therefore higher precipitation drag.
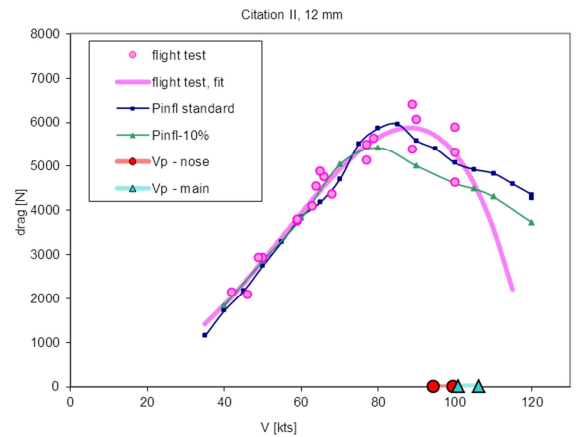

Fig. 6. Effect of reduced tyre pressure.

If the tyre pressure is lowered, not only the hydroplaning velocity is reduced, as indicated in

figure 6 by the symbols along the x-axis. The pressure in both the nose tyre and the main tyre was reduced. This results in a decrease in precipitation drag close to and above hydroplaning, due to the flattened spray.
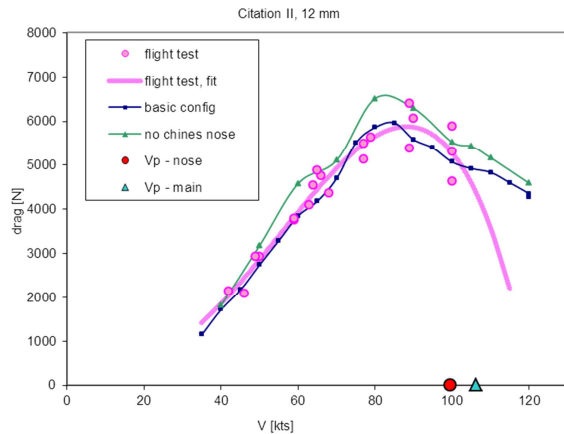

Fig. 7. Citation II: influence of chines

The nose tyre of the Citation is equipped with chines to reduce engine ingestion and precipitation drag. The effectiveness of these chines is clear from figure 7. Without chines there is significantly more spray impingement on the aircraft. Even more important: without chines the engine ingestion increases from a low level of 1.6 kg/s to around 10 kg/s.
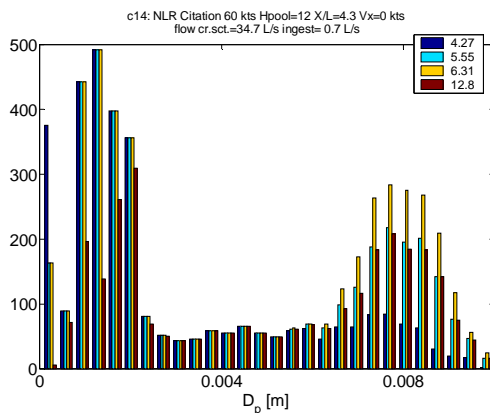
Fig. 8. Typical distribution of particle size at 4 X-positions (Citation, 60 kts, nose tyre spray)

Earlier it was mentioned that the particle sizes in the spray are typically in the range between 0.5 and 10 mm. Figure 8 shows the particle size distribution for the spray of the Citation at 4

different cross sections between stations just in front of the wing (X=4.27) and at the tail of the aircraft (X=12.8, see figure 3). The majority of particle sizes lies around 1 mm. A second 'hump' occurs at particle sizes around 8 mm. The smallest particles are generated in the bow wave in front of the tyre as the atomization effect is largest here. The larger particles are generated at increasing distance behind the tyre. This explains the maximum found for X=6. At the tail position, part of these particles have fallen back to the ground, not alone due to particle weight, but also due to their low initial velocity. This reduces the number of large particles counted in this cross section. Most particles reaching the engine originate from the bow wave and initial side wave region and therefore are of order 1 mm in size.
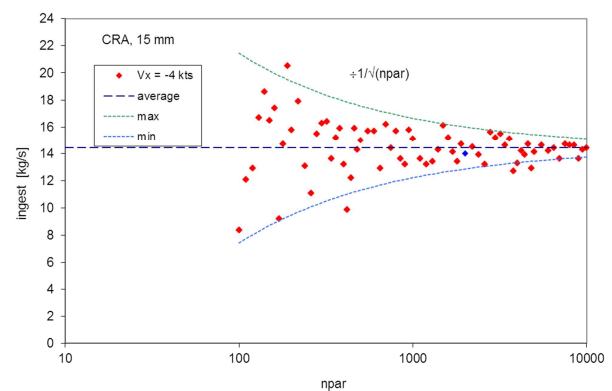

Fig. 9. Dispersion in ingestion rate as function of the number of particles used in the spray calculation for each side spray.

3.2   Engine ingestion

To obtain sufficient accuracy for engine ingestion, more particles are required for the simulation than is the case for precipitation drag. Figure 9 shows the dispersion in ingestion level for a varying number of particles. This result is obtained for a generic executive aircraft, slightly larger than the Citation and comparable e.g. to the Falcon 2000. This generic aircraft is designated 'CRA' (Contaminated Runway Aircraft). The figure shows that 5000 particles per side spray are required to obtain ingestion values within 1 kg/s or 7% of the average value. All calculations for

this aircraft have therefore been performed with this number of particles.
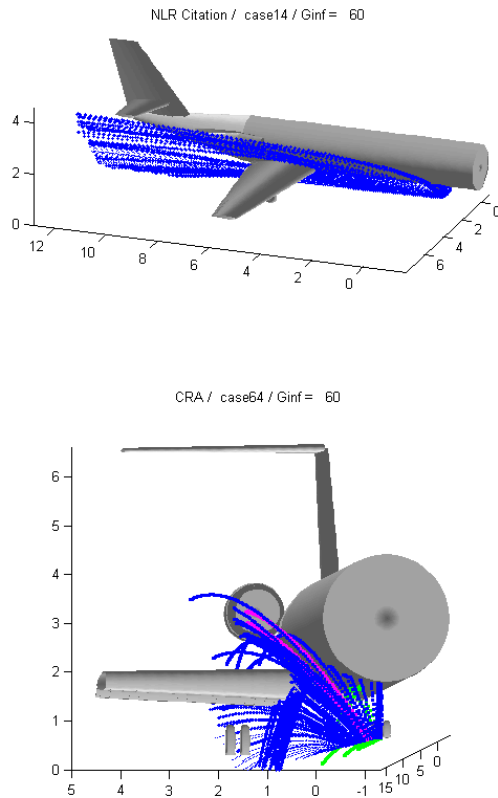

Fig. 10. CRA-aircraft: spray caused by the nose gear at 60 kts and a slight crosswind component of 4 kts towards the aircraft on the side where the engine is located.

The aircraft is equipped with side-by-side tyres both for the nose gear as well as for the main gear. The nose gear has 14.5x5.5 tyres without chines; the main gear has 26x6.6 tyres. All tyres are cross-ply and the distance between the pair of nose tyres and main tyres amounts to 0.24 m and 0.30 m respectively. The nose and main tyre are inflated to 11.1 and 13.5 bar respectively.

Figure 10 shows a typical spray pattern around the CRA aircraft from two different viewing angles. Dimensions along the axes are in meters. The reflection of the spray on the wing is clearly visible in the second view. Pool depth used for the CRA equals 15 mm. Only the nose gear is causing ingestion. The spray from

the main gear does not reach the engine, due to the shielding effect of the wing. Therefore this part of the spray is not shown. Aircraft weight equals 20000 lbs. The green trajectories are centre spray trajectories and the pink trajectories are those that are ingested by the engine. Note that only a limited number of the actual 5000 trajectories being calculated is shown in these figures for clarity.

3.3 Crosswind effects

The question arises whether crosswind may affect the position of the spray in such a way that ingestion is increased significantly. If a crosswind occurs, the resulting ingestion rates for the generic CRA geometry are shown in figure 11. Negative values of V_x correspond to a crosswind forcing the spray towards the fuselage-mounted engine.
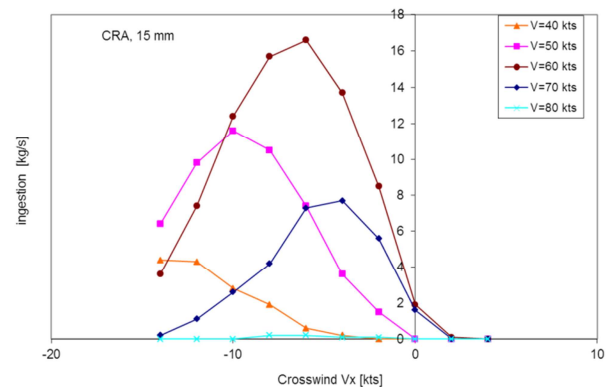

Fig. 11. CRA: ingestion rates as function of cross wind velocity for various rolling speeds.

Without cross wind the ingestion remains very limited to around 2 kg/s at ground speeds of 60 to 70 kts. These levels quickly increase for negative cross winds. The maximum ingestion occurs for a speed of 60 kts and amounts to 16.6 kg/s. For lower speeds the required crosswind to obtain maximum ingestion becomes larger. In that case the spray is located more outboard and therefore a large crosswind is required to cause ingestion. Figures 12 and 13 show the flow distributions in the various sprays in a cross section coinciding with the engine intake.
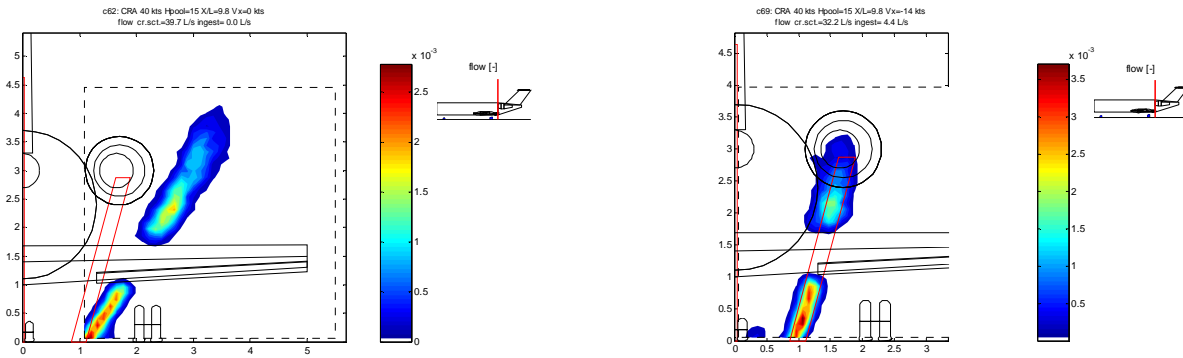
a. ground speed 40 kts

a. ground speed 40 kts, V_X = 14 kts
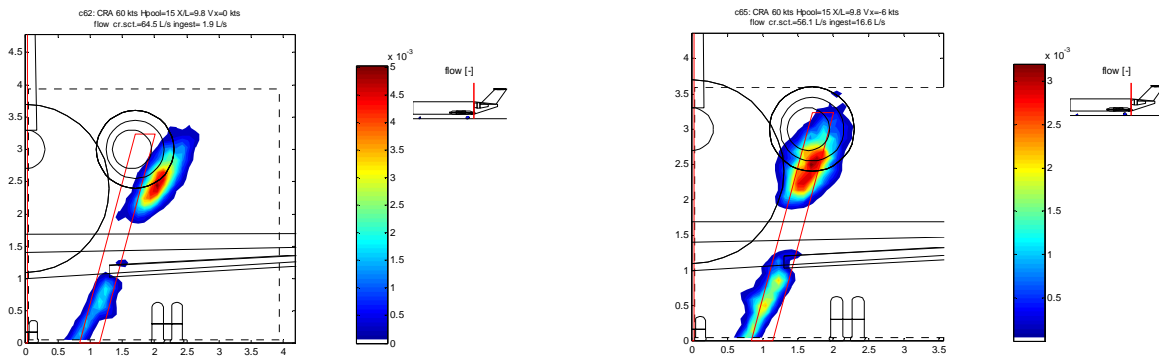
b. ground speed 60 kts

b. ground speed 60 kts, V_X = 6 kts

Fig. 12. CRA spray without cross wind

Fig. 13. CRA spray with a crosswind

Often nose tyres are equipped with chines. In case of chines the ingestion rates become lower and also the maximum ingestion occurs at higher crosswind velocities. Figure 14 shows the results for a ground speed of 60 kts. Note that without crosswind the ingestion rate with chines equals almost zero. This means that an ingestion free test at zero crosswind does not guarantee that ingestion does not occur for unfavorable crosswinds! This should be born in mind when judging water through tests. A thorough evaluation of crosswind risks cannot be circumvented.

Of course the question remains whether the levels of ingestion found are acceptable. This depends on the engine characteristics and will be specified by the engine manufacturer. A typical engine in the 'CRA category' could be the TFE-731 having a maximum thrust of 16.5 kN. This thrust corresponds to a mass flow of around 55 kg/s. In flight engine operation requirements typically specify a water/air ingestion mass flow ratio of 4% at which no hazardous loss of power may occur (e.g. [3]). This means that a water ingestion rate of 17 kg/s, corresponding to 30%, almost certainly will be unacceptable for the engine.
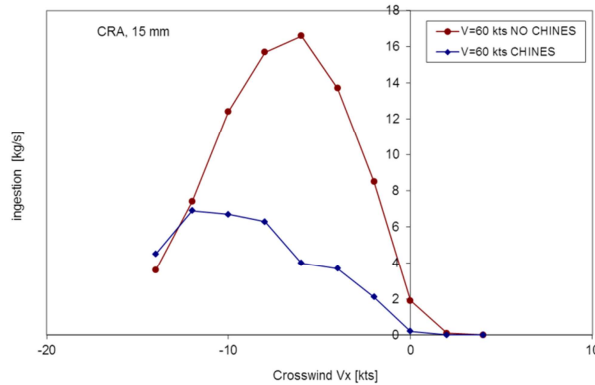
Fig. 14. CRA: ingestion lowered by nose tyre equipped with chines, ground speed 60 kts.

4 Conclusion

A method for calculating the effect of a water spray generated by tyres on a contaminated runway has been developed. The method allows calculating the effects of various parameters on the aircraft drag and engine ingestion and has proven to be a useful tool for this purpose. It is shown that crosswind may give rise to high engine ingestion levels, depending on the aircraft ground speed. High engine ingestion may lead to a flame-out in the worst case and represents a critical situation, especially as precipitation drag is already extending the take-off roll. For tail mounted engines the windward engines will be at risk in this respect. It is also shown that zero ingestion at low wind speeds in no guarantee for low ingestion at even moderate crosswind velocities.

References

[1] Supplementary performance information for take-off from wet runways and for operations on runways contaminated by standing water, slush, loose snow, compacted snow or ice, *JAR 25. AMJ 25X1591* 1993.

[2] *Certification specifications and acceptable means of compliance for large aeroplanes CS-25.* Amendment 11, July 2011, EASA

[3] *Certification specifications for normal, utility, aerobatic, and commuter category aeroplanes.* CS-23, 2010. EASA

[4] FAA. Water ingestion testing for turbine powered airplanes. *FAA AC 20-124*, 1985.

[5] ESDU. Estimation of spray patterns generated from the sides of aircraft tyres running in water or slush. *ESDU 83042*, 1998.

[6] Daugherty R.H., Stubbs S.M.. Measurements of flow rate and trajectory of aircraft tire-generated water spray *NASA TP 2718*, 1987.

[7] Barrett R.B.. Drag and spray measurements from a pair of small pneumatic tyres placed side by side, *Ministry of Aviation, S&T Memo 8/64*, 1965.

[8] Barrett R.B.. Drag and spray measurements from a small pneumatic tryre travelling through a water layer. *Ministry of Aviation, S&T Memo 11/63*, 1963.

[9] Wolff J.M., Renee G., Existing data analysis (Dassault) *EU Contamrunway Deliverable D4*, Dassault Aviation, 1997.

[10] Andersson A., Existing data analysis turboprops. *EU Contamrunway Deliverable D3*, Saab AB, 1997.

[11] Giesberts M. Precipitation drag measurements obtained in a pond for a Citation II. *NLR TR 97574 L*, 1997.

[12] Giesberts M., Gooden J.H.M., Precipitation drag of snow and standing water, paper, *ICAS 2000*

[13] Sirignano W.A. *Fluid Dynamics and Transport of Droplets and Sprays*. Cambridge University Press, 1999.

[14] Kolev N.I. *Multiphase flow dynamics: thermal and mechanical interactions*, Springer, 2007.

[15] Guildenbecher D.R., López-Rivera C., Sojka P.E., Secondary atomization Review article *Exp.in Fluids*, vol 46, pp.371-402, 2009.

[16] Pruppacher H.R., Klett J.D. *Microphysics of clouds and precipitation*, Springer, 1997.

[17] Tokay A., Kruger A., Krajewski W.F., Kucera P.A., Filho A.J.P. Measurements of drop size distribution in the southwestern Amazon basin. *J.Geophysical Research*, vol.107, 2002.

[18] Bragg M.B., A similarity analysis of the droplet trajectory equation. *AIAA 82-4285*, 1982.

[19] ESDU. Frictional and retarding forces on aircraft tyres. Part V: estimation of fluid drag forces. *ESDU 90035*, 1990.

[20] Gooden J.H.M. CR*spray* – Impingement drag calculation of aircraft on water-contaminated runways. *48th CASI Anual Conference*, Toronto, May 2001.

[21] Leland T.J.W., Taylor G.R. An investigation of the influence of aircraft tire-tread ware on wet-runway braking, *NASA TN D-2770*, 1966.

Copyright Statement